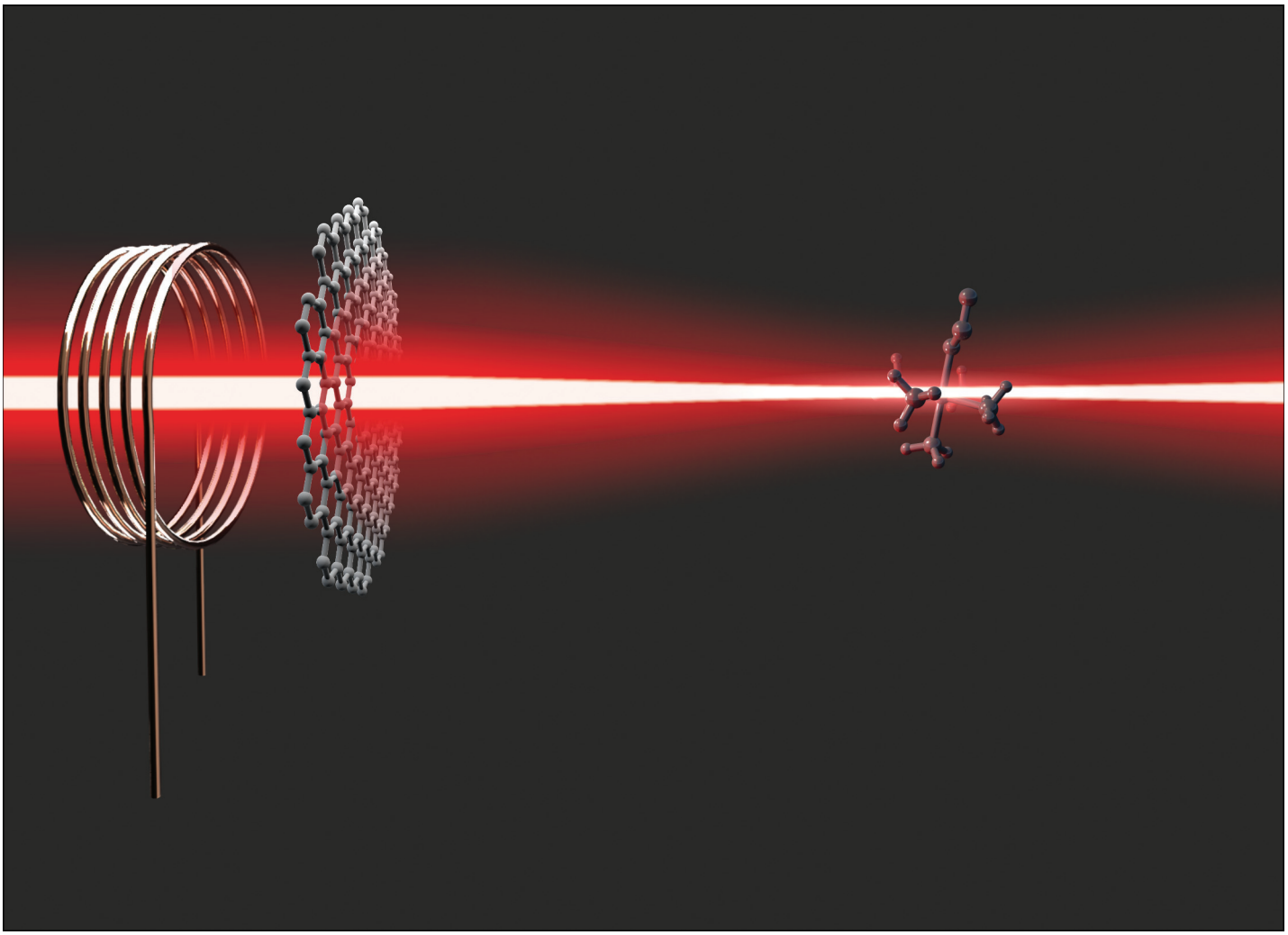

Showcasing research from the FREIA Laboratory of Uppsala University (Sweden); School of Radio Physics, V. N. Karazin Kharkiv National University (Ukraine); and Donostia International Physics Center (Spain).

Optical magnetic lens: towards actively tunable terahertz optics

It is shown analytically and numerically that 2D materials immersed into a non-uniform, specially profiled magnetic field can focus terahertz light. This finding opens the door to novel magnetically-tunable 2D lenses for ultrafast applications.

As featured in:

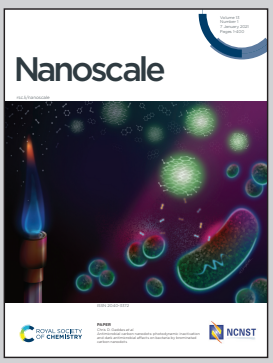

See Alexey Y. Nikitin, Vitaliy Goryashko *et al.*, *Nanoscale*, 2021, **13**, 108.

ROYAL SOCIETY OF CHEMISTRY

rsc.li/nanoscale

Registered charity number: 207890

Nanoscale

PAPER

View Article Online
View Journal | View Issue

Check for updates

Cite this: *Nanoscale*, 2021, **13**, 108

Optical magnetic lens: towards actively tunable terahertz optics†

Georgii Shamuilov,[a] Katerina Domina,[b,c] Vyacheslav Khardikov,[b,c] Alexey Y. Nikitin *[d,e,f] and Vitaliy Goryashko *[a]

As we read this text, our eyes dynamically adjust the focal length to keep the image in focus on the retina. Similarly, in many optics applications the focal length must be dynamically tunable. In the quest for compactness and tunability, flat lenses based on metasurfaces were introduced. However, their dynamic tunability is still limited because their functionality mostly relies upon fixed geometry. In contrast, we put forward an original concept of a tunable Optical Magnetic Lens (OML) that focuses photon beams using a subwavelength-thin layer of a magneto-optical material in a non-uniform magnetic field. We applied the OML concept to a wide range of materials and found out that the effect of OML is present in a broad frequency range from microwaves to visible light. For terahertz light, OML can allow 50% relative tunability of the focal length on the picosecond time scale, which is of practical interest for ultrafast shaping of electron beams in microscopy. The OML based on magneto-optical natural bulk and 2D materials may find broad use in technologies such as 3D optical microscopy and acceleration of charged particle beams by THz beams.

Received 27th August 2020,
Accepted 9th November 2020

DOI: 10.1039/d0nr06198k

rsc.li/nanoscale

Open Access Article. Published on 11 November 2020. Downloaded on 2/22/2021 9:58:49 AM.
This article is licensed under a Creative Commons Attribution-NonCommercial 3.0 Unported Licence.

The lens as a tool for focusing transmitted light has been around for four thousand years.[1] It imprints a proper phase shift onto a light wavefront making the wavefront converging. Conventional optical components (lenses, waveplates, prisms) are *optically thick*,[2] and rely on their geometry to imprint required phase shifts by means of the difference in refractive indices. This approach faces a fundamental limitation: the lack of transparent materials with a high contrast of indices of refraction (a higher index of refraction implies lower transparency because of the Kramers–Kronig relations).

In contrast, a new field of *planar* or *flat optics* has been thriving for the past decade. The concept consists in imprinting abrupt, controlled phase shifts onto transmitted light by a 2D array of subwavelength-thin nanoresonators, metasurface.[3–10] Thus, planar optical components can be made *nanometre thin* and comply with industrial lithography fabrication.

One of the desired functionalities of both conventional and planar lenses is the active tunability of focal length: think of the eye. Nature's solution realised in mammals' eyes is to tune the focal length by changing the curvature of the lens with the

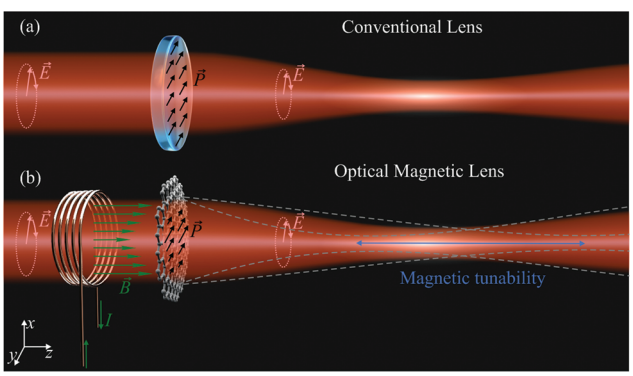

Fig. 1 Focusing of a photon Gaussian beam with an electric field $\vec{E}$ by a lens. Both the geometry and medium polarisation $\vec{P}$ of refractive lens (a) govern the cumulative phase shift of the transmitted beam wavefront. In the OML (b), the phase shift is solely due to non-uniform $\vec{P}$, which however depends on the transverse profile of the magnetic field $\vec{B}(\vec{r})$ provided by the coil. Thus, in the OML the wavefront can be controlled *via* $\vec{B}(\vec{r})$. Dashed lines show the envelopes of the focused photon beam for different magnetic field curvatures and the blue arrow indicates the change of the waist location.

[a]*Department of Physics and Astronomy, Uppsala University, Lägerhyddsvägen 1, Uppsala, 75120, Sweden. E-mail: vitaliy.goryashko@physics.uu.se*
[b]*School of Radio Physics, V. N. Karazin Kharkiv National University, 4, Svobody Square, Kharkiv 61022, Ukraine*
[c]*Institute of Radio Astronomy of National Academy of Sciences of Ukraine, 4, Mystetstv Street, Kharkiv 61002, Ukraine*
[d]*Donostia International Physics Center (DIPC), 20018 Donostia-San Sebastián, Spain. E-mail: alexey@dipc.org*
[e]*IKERBASQUE, Basque Foundation for Science, 48013 Bilbao, Spain*
[f]*CIC nanoGUNE BRTA, Tolosa Hiribidea 76, E-20018 Donostia-San Sebastián, Spain*
†Electronic supplementary information (ESI) available. See DOI: 10.1039/D0NR06198K

This journal is © The Royal Society of Chemistry 2021

Open Access Article. Published on 11 November 2020. Downloaded on 2/22/2021 9:58:49 AM.
This article is licensed under a Creative Commons Attribution-NonCommercial 3.0 Unported Licence.

ciliary muscle and by employing a slight gradient of the index of refraction.[11] A number of eye-inspired approaches and metasurface-based methods have been demonstrated using mechanical or electric control.[12–24] Meanwhile, active ultrafast and wide tunability is still challenging.[13]

At the same time, actively tunable lenses have been used for around a century in electron microscopy to focus *charged particle beams* by spatially non-uniform magnetic fields. However, magnetic focusing does not apply to chargeless photon beams. In this article, we put forward an original concept of an Optical Magnetic Lens (OML) that focuses *photon beams* using a subwavelength-thin layer of a magneto-optical material immersed into a *non-uniform magnetic field*, sec. I. We set forth the physics of the OML and exemplify its performance in different frequency bands with bulk and 2D materials, sec. II.

The OML features *tunability* of the focal length *via* changing the strength or curvature of the magnetic field. Specifically, the wavefront of an optical beam incident onto the OML receives a phase shift according to the transverse distribution of the magnetic field strength (Fig. 1). The effect is the most profound in the vicinity of cyclotron resonance in the chosen material, with a phase shift up to one rad, resulting in cm-scale focal distances. An analysis of the practical realisation of the OML shows that a quite simple experimental setup can be used to test the OML concept, sec. III.

I. Brief theory

To illustrate our concept, let us examine the transformation of a Gaussian optical beam by the OML. Consider a subwavelength-thin, infinitely wide, flat layer of an isotropic medium, supporting free charges. The layer is immersed into an axially symmetric, static, non-uniform magnetic field B. The magnetic field is normal to the layer and its strength varies quadratically with distance in the medium [such as the field of a coil or ring, see Fig. 1]. Let the origin of a Cartesian coordinate system (x, y, z) be aligned with the extremum of the magnetic field in the layer and the z-axis being normal to the layer. A Gaussian optical beam is normally incident onto the layer with the beam waist positioned in the layer: $\vec{E} = \vec{E}_0 e^{-(x^2+y^2)/w_0^2}$. Here, $\vec{E}_0$ and w_0 are the amplitude and waist, respectively. A sinusoidal behaviour in time at frequency ω is assumed.

We treat the layer as an anisotropic medium with its charge carriers oscillating in the combined optical and static magnetic field. Solving the equations of motion for charge carriers in the layer and relating the electric current to the electric field, we find the tensor of dielectric permittivity [see ref. 25 and ESI (D)†]

$$\hat{\varepsilon} = \begin{pmatrix} 1+\varepsilon_\perp & -i\beta & 0 \\ i\beta & 1+\varepsilon_\perp & 0 \\ 0 & 0 & \varepsilon_\parallel \end{pmatrix} \quad (1)$$

where $\varepsilon_\perp$ differs from the convention by unity to shorten coming derivations. The elements of this tensor are functions of $r = \sqrt{x^2+y^2}$ because the static magnetic field depends on r as $B = B_0 p(r)$, with B_0 being the field amplitude and $p(r)$ the radial profile. For field inhomogeneity small on the wavelength scale, $\lambda d(\log p)/\mathrm{d}r < 1$, with λ being the wavelength, the functional form of $\hat{\varepsilon}$ remains unchanged [see ESI (D)†].

The electric field of the Gaussian beam propagating through the layer in the positive z direction is governed by the inhomogeneous paraxial wave equation[26]

$$(\Delta_\perp + 2ik\partial_z)\vec{E} = -k^2(\hat{\varepsilon} - \hat{I})\vec{E}, \quad (2)$$

where $\hat{I}$ is the unit tensor, $k \equiv 2\pi/\lambda = \omega/c$ is the wave number, c is the speed of light, $\Delta_\perp$ and ∂_z are the transverse Laplacian and the partial derivative along z, respectively. Thanks to the rotational symmetry of the problem with respect to the z-axis, left-handed (LH) and right-handed (RH) circularly polarised waves are eigenmodes of the problem. In other words, LH and RH waves are decoupled from each other and can be analysed separately. Hereinafter, all results are derived and illustrated for circularly polarised waves. We introduce LH, subscript +, and RH, subscript −, circularly polarised waves as $E_\pm = E_x \pm iE_y$. Then, the paraxial wave equation splits and takes on the scalar form

$$(\Delta_\perp + 2ik\partial_z)E_\pm = -k^2(\varepsilon_\perp \mp \beta)E_\pm. \quad (3)$$

Outside the layer, the longitudinal field component E_z can be found from the Coulomb law $\vec{\nabla}\cdot\vec{E} = 0$.

The reflected Gaussian beam propagating in the negative z direction is described by the same paraxial equation as (3) with the only difference that the wavenumber k must be replaced by $-k$. As usual in electrodynamics, the boundary conditions consist in the continuity of the electric field $E_\pm$ and its derivative with respect to the propagation coordinate z.

Since the layer is subwavelength thin, diffraction can be safely disregarded and the mathematical problem becomes essentially one-dimensional. The analytical solution for reflected and transmitted waves is described in terms of reflection, $\mathcal{R}$, and transmission, $\mathcal{T}$, Fresnel coefficients, respectively. Namely, the electric field of the transmitted optical beam reads as $E_\pm = \mathcal{T}E_{0,\pm}e^{-r^2/w_0^2}$. For normal incidence, the Fresnel coefficients take on a simple and well known form[27]

$$\mathcal{T}_\pm = \frac{1}{1+\alpha_\pm}, \mathcal{R}_\pm = \frac{-\alpha_\pm}{1+\alpha_\pm}, \alpha_\pm = -\frac{i\pi d}{\lambda}(\varepsilon_\perp \mp \beta), \quad (4)$$

under the assumption that $|\alpha_\pm| \ll 1$. General formulas for arbitrary incidence angles can be found, for example, in ref. 28. The important result is that the Fresnel coefficients locally depend on the transverse coordinate *via* the non-uniform magnetic field.

For a 2D material with conductivity $\sigma_\pm$, the parameter $\alpha_\pm$ is simply the normalised conductivity: $\alpha_\pm = (2\pi/c)\sigma_\pm$. Furthermore, for a 2D material the coefficients $\mathcal{T}_\pm$ and $\mathcal{R}_\pm$ in eqn (4) are exact for any value of $\alpha_\pm$. Note that it is common to describe 2D materials by a conductivity tensor but we choose to use the permittivity tensor to unify the notations for 2D materials and thin layers of bulk materials.

Open Access Article. Published on 11 November 2020. Downloaded on 2/22/2021 9:58:49 AM.
This article is licensed under a Creative Commons Attribution-NonCommercial 3.0 Unported Licence.

The Fresnel coefficients in eqn (4) depend on a local static magnetic field, $\mathcal{R}_\pm[B(r)]$, $\mathcal{T}_\pm[B(r)]$, thus setting the spatial phase profile of the reflected and transmitted electromagnetic fields of the beam. The *inhomogeneous phase shift* $\varphi_\pm = \arg\{\mathcal{T}_\pm[B(r)]\}$ in eqn (4) impacts the shape of the transmitted wavefront. In particular, a quadratic profile of the magnetic field

$$p(r) = 1 + \frac{r^2}{{R_c}^2}, \frac{r}{R_c} \ll 1 \tag{5}$$

with R_c being the radius of curvature, gives the focusing effect. To see the focusing explicitly, we compare the phase shift of the OML to that of a conventional lens, $\delta\varphi = kr^2/(2f)$, where f is the focal length. To simplify $\varphi_\pm$, we Taylor expand it with respect to (r/R_c) as

$$\varphi_\pm = \varphi_\pm|_{r=0} + \frac{1}{2}\varphi''_\pm|_{r=0}\frac{r^2}{{R_c}^2}, \tag{6}$$

with $\varphi''_\pm$ being the second derivative of $\varphi_\pm$. Similarly to $\delta\varphi$, the inhomogeneous phase shift of the OML scales quadratically with r [second term in eqn (6)], thus clearly indicating a focusing effect. By comparing the expanded $\varphi_\pm$ with $\delta\varphi$, we find the focal length of the *tunable flat OML* for LH and RH circularly polarised waves

$$f_\pm = \frac{k{R_c}^2}{\varphi''_\pm}. \tag{7}$$

Image formation by the lens is well known in optics and discussed in ESI (B)† for completeness.

Examine the contents of results (4) and (7). First, the homogeneous part of the phase shift $\varphi_\pm$ leads to the Faraday rotation of *linearly* polarised light. Second, within the layer, the left and right circularly polarised components of the electric field experience different effective permittivities $\alpha_\pm$, and the focal length (7) contains different signs. Thus, the polarisation components have different focal lengths. Third, a comparison with full-wave simulations showed that the solution (7) is accurate under a constraint of $w_0 < 2R_c$, more relaxed than the one in eqn (5). Fourth, the reflectivity of the layer can be high and thus allows for OML operation in reflecting telescope or mirror geometry.

To obtain an explicit expression for $f_\pm$ as a function of parameters of the film, let us proceed to the elements of the tensor $\hat{\varepsilon}$, eqn (1). The charges oscillate around the applied magnetic field with a frequency $\omega_c(r) = \omega_0\mathcal{M}p(r)$. Here, $\omega_0 = qB_0/m_e c$ is the reference (on-axis) cyclotron frequency with m_e being the electron mass, $\mathcal{M} = m_e/m^*$ is the mass reduction ratio, q and m^* are the charge and effective mass of the particle, respectively. In fact, the elements of the tensor $\hat{\varepsilon}$ correspond to a magnetised plasma (Drude model)[29–31] and read

$$\varepsilon_\perp = \frac{-\mathcal{A}(\omega - i/\tau)}{\omega\left[(\omega - i/\tau)^2 - {\omega_c}^2(r)\right]}, \beta = \frac{\omega_c(r)\varepsilon_\perp}{(\omega - i/\tau)}, \tag{8}$$

where $\mathcal{A}$ is a material-specific constant [s^{-2}] and τ is the relaxation time. Particular cases with more familiar expressions for $\varepsilon_\perp$ and β can be found in ESI (A).† Following eqn (4), we obtain a simple expression for the focal length for LH and RH circularly polarised waves transmitted through a layer of thickness d as

$$f_\pm = \mp\frac{{R_c}^2}{\mathcal{A}d}\frac{\omega}{\mathcal{M}\omega_0}\frac{[(\omega \mp \mathcal{M}\omega_0)^2 + (1/\tau)^2]^2}{(\omega \mp \mathcal{M}\omega_0)^2 - (1/\tau)^2}. \tag{9}$$

This simple result allows one to calculate the focal length of the OML for different materials as illustrated below. Due to the term $(\omega \mp \mathcal{M}\omega_0)^2$ in the denominator in eqn (9), $f_\pm$ has a resonant behaviour for one of the polarisations of the optical beam for a given magnetic field orientation. Specifically, for a longitudinal magnetic field oriented along the positive direction of the z-axis, the cyclotron resonance, $\omega \approx \mathcal{M}\omega_0$, occurs for the LH circularly polarised optical beam E_+. In general, at the resonance eqn (9) simplifies to $f_\pm \approx \mp{R_c}^2/(\mathcal{A}d\tau^2)$.

II. Examples of materials

Consider potential practical realisations of the OML for different frequency bands.

Materials suitable for magnetic focusing in the microwave range are *magnetic dielectrics*, or *ferrites*, such as Yttrium Iron Garnet (YIG). Instead of charge carriers, there are unpaired spins precessing in the applied magnetic field. The functional form of $\hat{\varepsilon}$, eqn (1), and its components remain unchanged. Hence, the result in eqn (9) can be applied directly to ferrites, where ω_0 should be understood as the Larmor frequency [see ESI (A)†].[32] Practical results for the OML in the microwave region are presented in Table 1. A focal length of tens of centimeters is feasible. Ferrite-coated mirrors can potentially be used for *tunable* focusing of quasi-optical microwave beams in fusion experiments, *e.g.* for plasma probing or electron-cyclotron-resonance heaters.[33,34]

To operate above microwaves, we need a material with a high mass reduction factor $\mathcal{M}$, $\mathcal{M} \gg 1$. *Doped graphene* is an outstanding candidate for a higher-frequency OML. We use the semiclassical model to describe doped graphene in magnetic fields.[35] This model accounts only for intraband transitions, but is valid in a broad range covering the terahertz and mid-infrared bands under the condition $\hbar\omega < 3|\mu_c|$.[35] Here, μ_c is the chemical potential and $\hbar$ is the reduced Planck constant.

Table 1 Examples of materials for optical magnetic lens in transmission mode (T) at normal incidence $\varphi_i = 0$ and in reflection mode (R) at $\varphi_i = 20°$. For InSb, THz phonon resonances must be avoided

Parameter	Graphene (T)	Graphene (R)	InSb (T)	InSb (R)	YIG (T)
Light frequency $\omega/2\pi$	1 THz	1 THz	3 THz	2 THz	50 GHz
Relaxation time τ	0.5 ps	1 ps	3 ps	3 ps	≈0.1 μs
Efficiency ($\lvert T\rvert^2$ or $\lvert R\rvert^2$)	32%	55%	27%	66%	72%
On-axis field B_0	0.2 T	0.2 T	2.1 T	1.7 T	1.8 T
Field curvature R_c	0.32 cm	0.3 cm	1.5 cm	1.5 cm	70 cm
Film thickness d	Monolayer	Monolayer	0.6 μm	3 μm	0.1 μm
Focal length f	8 cm	40 cm	16 cm	40 cm	51 cm

This journal is © The Royal Society of Chemistry 2021

Open Access Article. Published on 11 November 2020. Downloaded on 2/22/2021 9:58:49 AM.
This article is licensed under a Creative Commons Attribution-NonCommercial 3.0 Unported Licence.

To use eqn (9) directly for a graphene sheet with a conductivity $\hat{\sigma}$, we approximate graphene by a layer with a finite thickness d and introduce an effective dielectric permittivity tensor $\hat{\varepsilon}_{\text{eff}} = (4\pi i/\omega d)\hat{\sigma}$.[27] Then, the elements of $\hat{\varepsilon}_{\text{eff}}$ assume the form given by eqn (8). As it should be for a 2D material, the dependence on d in $f_{\pm}$ cancels out. For doped graphene, $\mathcal{M}$ is $m_e V_F^2/|\mu_c|$. We see that graphene poses an intriguing possibility of increasing the mass reduction factor M by increasing the Fermi velocity v_F and operating with a small chemical potential μ_c. From the practical point of view this implies that the cyclotron resonance can be reached for lower magnetic fields for the same THz frequency. Recent experiments in the THz and IR regions show that the Fermi velocity can be engineered by placing graphene on a suitable dielectric substrate.[36,37] Assuming a chemical potential μ_c = 0.19 eV and Fermi velocity V_F = 2.5·10^6 m s^{-1}, we estimate $\mathcal{M} \approx 187$ and $\mathcal{A} \approx 1.2 \times 10^{18}\text{s}^{-2}$. The remaining parameters are listed in the Table 1.

Let us take a closer look at the optical response of a graphene layer in a *uniform* magnetic field. First, we recall that for a longitudinal magnetic field oriented along the positive z-axis, the LH circularly polarised optical beam E_+ exhibits a cyclotron resonance, see eqn (9). This is illustrated in Fig. 2, which shows a clear resonant behaviour of the transmitivity, reflectivity and phase shifts at the cyclotron resonance of 0.2 T. The distributions in the figure remain exactly the same for the *RH* circular polarisation for a *reversed* direction of the magnetic field due to the problem symmetry. The maximum of the derivative of the phase shift with respect to the magnetic field, $\mathrm{d}\varphi/\mathrm{d}B_0$, suggests an operating point of the OML in a *non-uniform* magnetic field. Namely, for $B_0 \approx 0.2$ T, $\mathrm{d}\varphi/\mathrm{d}B_0$ is maximal, and the graphene OML would attain the minimal value of f_+ in a *non-uniform* field, given that other parameters are fixed. One should keep in mind that the OML focusing effect is dictated by the form of the spatial distribution of the magnetic field whereas the cyclotron resonance can only enhance the focusing effect but does not change its nature. The inverse relaxation time of graphene, $1/\tau$, plays the role of the resonance bandwidth: larger values of τ (high-purity graphene) provide a sharper resonance and thus a larger phase shift (on the order of one radian). At the same time, the OML appears tolerant to smaller τ values so that the graphene OML does not require high-quality graphene flakes for its reasonable performance.

For practical applications, the cyclotron frequency for graphene can be written in the engineering form as

$$\nu(\text{Hz}) = \frac{V_F^2(\text{m s}^{-1})}{2\pi}\frac{B_0(T)}{|\mu_c|(\text{eV})}. \tag{10}$$

The behaviour of ν *vs.* B_0 and $|\mu_c|$ for a representative set of parameters is shown graphically in Fig. 3.

For the resonant LH circular polarisation of the optical beam incident onto graphene OML, we calculate a focal length of some cm with a wide adjustment range given by the field amplitude B_0, Fig. 4b. Additional active adjustment of the focal length can be done by varying the chemical potential μ_c, Fig. 4a. Furthermore, f_+ can be tuned by adjusting the curvature of the magnetic field, for example, by using a combination of a permanent ring magnet and a tunable current coil. Thus, the OML can bring vast tunability into existing THz optics.

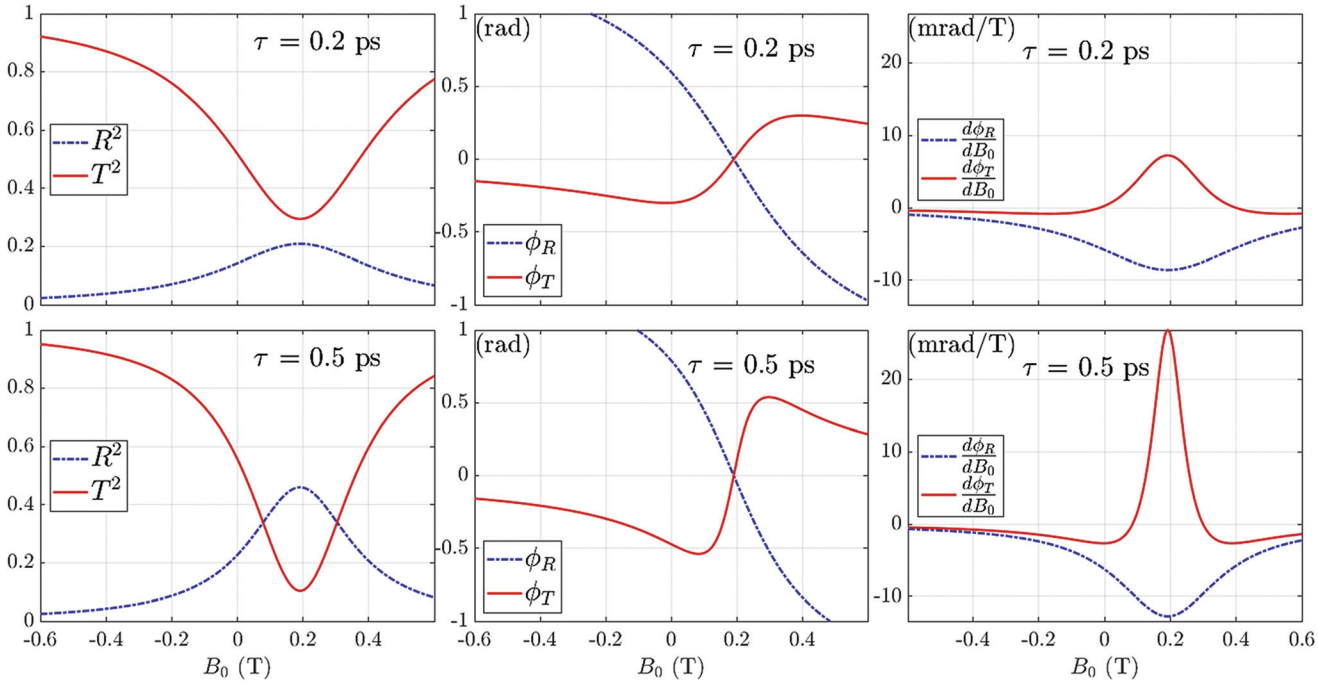

Fig. 2 Transmission, reflection, phase shift and derivative $\mathrm{d}\varphi/\mathrm{d}B_0$ of an LH circularly polarised optical beam calculated *via* Fresnel coefficients (4) for a graphene layer w.r.t. applied magnetic field B_0 (uniform). The chemical potential is 0.19 eV.

Open Access Article. Published on 11 November 2020. Downloaded on 2/22/2021 9:58:49 AM.
This article is licensed under a Creative Commons Attribution-NonCommercial 3.0 Unported Licence.

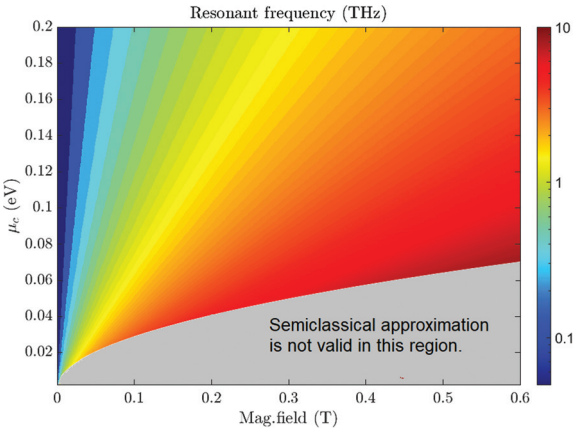

Fig. 3 Cyclotron frequency of graphene *vs.* the magnetic field and chemical potential. The shaded region is beyond the semiclassical approximation of the graphene conductivity used in the present model of OML.

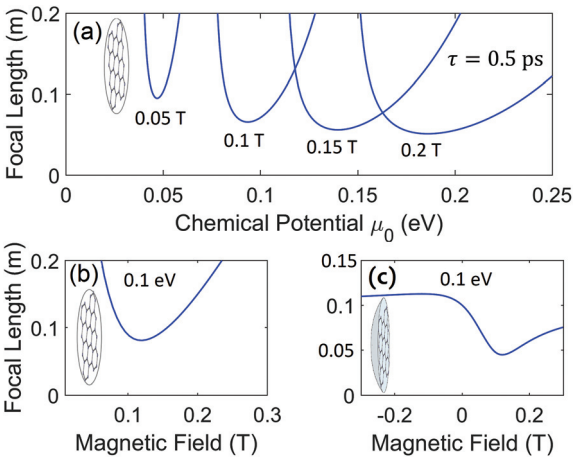

Fig. 4 (a) Focal length of graphene OML *vs.* chemical potential for different values of the magnetic field strength. (b) Focal length of graphene OML *vs.* applied magnetic field. (c) Focal length of a conventional lens *combined* with graphene OML *vs.* applied magnetic field. Here, τ = 0.5 ps, R_c = 3.2 mm, λ = 300 μm.

We note that only one circular polarisation component undergoes resonant focusing by the OML [$\omega \approx \mathcal{M}\omega_0$, see eqn (9) and ESI (A)†], while the other circular polarisation component is barely affected. Unlike other materials considered in this article, graphene exhibits a striking difference between LH and RH circular polarisations. Hence, such a lens allows for selective focusing by choosing the direction of the external magnetic field. This effect can be potentially used for polarisation-sensitive detection of THz light.

The OML can also be used in combination with conventional lenses, substantially improving the performance of the latter. As an example, Fig. 4c shows 50% relative tunability of a conventional lens, having a fixed focal length f of 10 cm, decorated with the graphene OML. The focal distance of the combined lens can be tuned from around 5 to 12 cm as the magnetic field goes through the cyclotron resonance at 0.1 T. For negative (non-resonant) values of the magnetic field, the OML tuning effect is negligible.

To visualise the effect of the OML as well as to cross-check our analytical results, we run full-wave simulations for the particular example of graphene OML. We use commercial software COMSOL Multiphysics. Thanks to the azimuthal symmetry of the problem, the model can be built in 2D to reduce required computation power. The incident Gaussian beam (background field) is defined analytically and the graphene layer is represented as a surface current density given by a 2D conductivity tensor.[27,31,35] The non-uniform magnetic field is included analytically *via* the components of the conductivity tensor.[31] The final field distribution is calculated as the field scattered by the graphene layer.

The focusing effect is clearly seen in Fig. 5. If no magnetic field is applied (lens is "off"), the Gaussian beam diverges in the region to the right from the graphene OML (top plot). In contrast, a new waist of the beam appears (bottom plot), when a profiled magnetic field is applied (lens is "on"). The focal lengths calculated analytically, 6.5 cm, and numerically, 6.4 cm, match very well, thus validating our analytical approach, eqn (1)–(9). The simulated transmission efficiency defined as the ratio of the transmitted power to the incident one is 42%.

In Fig. 5, for having a sharper image and clearer visual illustration, we partly compensated for lens aberrations by adding a term $-0.8r^6/R_c^6$ to the magnetic field profile $p(r)$. In the simulation, τ = 0.5 ps, μ_0 = 0.1 eV, B_0 = 0.09 T, $R_c = 1.2w_0$, $w_0 = 6\lambda$ with λ = 300 μm.

Semiconductors and their heterostructures are another important example of materials for the OML. The sophisticated underlying mechanism of charge transport significantly reduces the effective mass of electrons,[38,39] which can increase OML operating frequencies. The highest value of $\mathcal{M} \approx 50$ in this class of materials is achieved for indium antimonide (InSb).[40] Assuming parameters tabulated in ref. 41, we calculate $\mathcal{A} = 9.26 \times 10^{25}\text{s}^{-2}$ and the focal length of about 16 cm (see Table 1). Compared to graphene, tunability in InSb is limited to magnetic field only. Also, InSb exhibits phonon modes in the same frequency range suppressing resonant focusing at phonon frequencies.

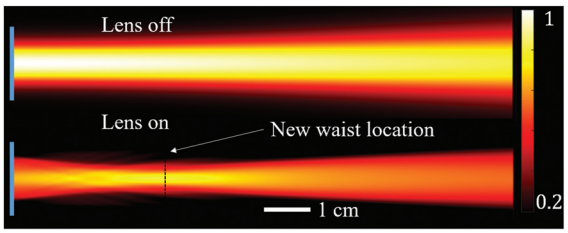

Fig. 5 Top plot: Normalised field distribution of the optical beam transmitted through the graphene OML *without* a non-uniform magnetic field (OML "off"). Bottom plot: Normalised field distribution with the OML "on".

This journal is © The Royal Society of Chemistry 2021

Open Access Article. Published on 11 November 2020. Downloaded on 2/22/2021 9:58:49 AM.
This article is licensed under a Creative Commons Attribution-NonCommercial 3.0 Unported Licence.

We also anticipate a possibility to use an array of *ferromagnetic nanoresonators* (*e.g.* TbCo[42,43]) for the OML at optical frequencies. Operating conditions are similar to those for ferrites discussed above. The focusing effect is weaker than in the THz range (the inhomogeneous phase shift is on the order of 10 mrad for $B_0 \sim 1$ T), but allows for fine-tuning of the focal length if the array is deposited on the surface of a plano-convex lens, similar to the example with graphene in Fig. 4c.

From a different perspective, the OML effect may impact propagation of electromagnetic waves in space similarly to a gravitational lens. Namely, a wavefront transformation may occur in *cosmic plasma* exposed to non-uniform magnetic fields generated by different massive astrophysical objects, thus affecting divergence of light from a remote source [see ESI (A)†].

III. Experimental considerations

Let us describe a possible experimental setup for focusing THz light with a graphene-based lens. Reduced to its essentials, the setup can consist of just four key components: (1) the lens itself: a transparent substrate decorated with large-scale doped graphene fabricated with chemical vapour deposition;[44] (2) a THz source based on optical rectification from, *e.g.*, a zinc telluride crystal[45] to generate an optical beam with a spectrum peaking at 1 THz; (3) a simple ring magnet to set the shape and focal length of the optical beam; (4) a THz beam imager based, for instance, on electro-optical sampling[45] or an array of microbolometers.[46] In practice, it is advantageous to place an additional thin current coil next to the ring magnet for fine tuning of the magnetic field curvature.

Note that the phase shift of the transmitted light $\varphi_\pm$ given by the Fresnel coefficient (4) is a complex function of B and hence a complex function of r. Hence, in the regime of strong focusing (large non-uniformity of the magnetic field) the optical quality of the proposed OML suffers from spherical aberrations if a simple quadratic profile of the magnetic field is applied. To correct for the aberrations, the transverse profile of the magnetic field must have not only a quadratic component (r^2), but also a component depending on r^6. For instance, in the simulation in Fig. 5 the optimal transverse profile of B is $(1 + r^2/R_c^2 - 0.8r^6/R_c^6)$. This profile can be realised in practice by properly choosing the longitudinal position of the graphene layer with respect to the ring magnet plane.

In Fig. 6, we show the magnetic field distribution for a typical commercial ring magnet. The transverse distribution of the longitudinal component of the magnetic field, Fig. 6b, changes with the longitudinal position. For certain longitudinal positions, close to the centre of the ring magnet, the magnetic field profile results in aberration-corrected focusing with the OML. In addition, a current coil can be used for fine tuning of the magnetic field profile.

For typical OML operation the radius of curvature of the magnetic field must be larger than the THz beam waist, $R_c \approx (1.2–1.3)w$. At the same time, for a ring magnet R_c is often smaller than the physical radius of the ring R, see Fig. 6. Hence, nearly 100% transmission of the THz beam through the aperture of the ring is possible since $R \approx 1.5w$. The typical numerical aperture is 0.1.

Thus, we have four different knobs in the OML magnet design to compensate for spatial aberrations: (i) the graphene layer position w.r.t. the ring magnet, (ii) the separation between the ring magnet and the current coil, (iii) the coil radius and (iv) the number of windings.

IV. Discussion

At THz frequencies, the response time of the graphene-based OML can potentially be as short as a few picoseconds. Though the physical mechanism of the phase shift induced in the

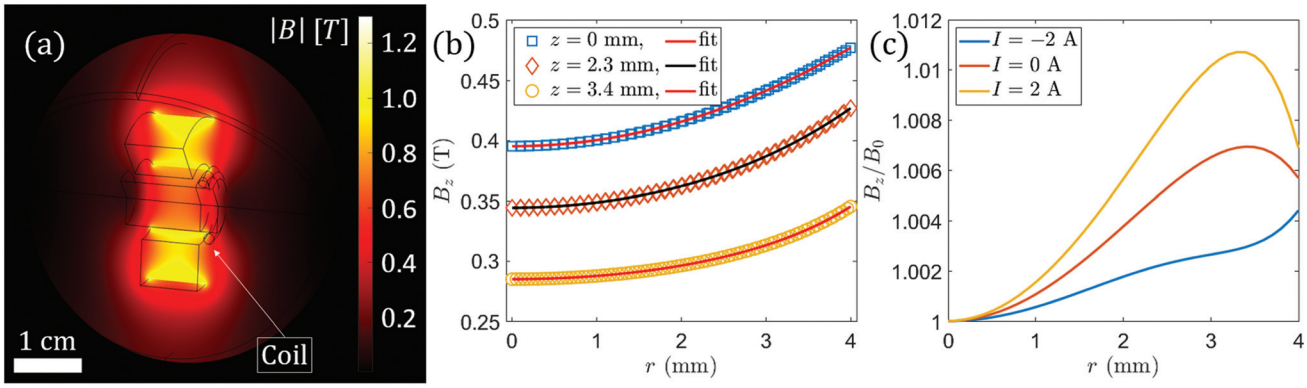

Fig. 6 Simulated spatial distribution of the magnetic field of a commercially available neodymium ring magnet. (a) Magnetic flux density (norm) distribution. A coil for correction is indicated as an example; (b) the relevant z-component of the magnetic field at different positions along z, fitted with 6th-order polynomials; the corresponding field curvatures R_c are 14.2, 15.7 and 18.8 mm, respectively; (c) field curvature profiles $p(r) = B_z/B_0$ for different current values in the example correction coil, the OML is at z = 4.5 mm. The ±2-A range corresponds to 40% relative dynamic tunability of the focal length (with relative detuning of the resonant frequency 0.4%).

Open Access Article. Published on 11 November 2020. Downloaded on 2/22/2021 9:58:49 AM.
This article is licensed under a Creative Commons Attribution-NonCommercial 3.0 Unported Licence.

OML is resonant and relies on cyclotron resonance, the relaxation time is typically less than a picosecond. That allows for ultrafast tuning. In practice, the response time will be limited by technical auxiliaries such as the response time of an electromagnetic coil used to create the required magnetic field profile. However, there is a promising solution for tuning the graphene-based OML on the picosecond time scale: to use quasi-half-cycle THz pulses[45,47] to additionally control the chemical potential, see Fig. 4a, and correspondingly adjust the focal length.

In contrast to sinusoidal electromagnetic pulses, quasi-half-cycle pulses maintain their electric field oriented in the preferential direction. Hence, the effect of such pulses on the graphene layer can be thought of as an instantaneous DC voltage. A permanent magnet can be used to preset a desired focal length of the OML and the electric field of an additional quasi-half-cycle THz pulse will modify the chemical potential on the picosecond time scale thus adjusting the focal length.

Compared to other tunable metalenses discussed in the literature, the OML offers (i) wide tunability of the operating frequency by one order of magnitude, see Fig. 3; (ii) 50% relative tunability of the focal length, see Fig. 4; (iii) the operating bandwidth of around 1 THz, see Fig. 2 and the discussion therein; and (iv) the transmission efficiency of 40%, see Fig. 5. To contrast our OML with other tunable metalenses, below we give a brief overview of the present state-of-the-art of the field. The existing designs of tunable metalens can broadly be divided into several classes. We consider representative examples from different classes irrespective of the frequency band since many designs can be extended to a longer wavelength regime.

In the class of *electro-mechanically* tunable lenses,[16,18,48] mechanically stretchable substrates are used in the lens design. For instance, an infrared metalens on a dielectric elastomer actuator[18] has a 100% relative tunability of the focal length. The reported response time is about 30 ms. In the near-infrared range, 130% focal length tuning is shown[16] with the response time similar to the above. In the microwave range, an inverse-designed stretchable metalens[48] allows for 75% relative tunability and about 70% transmission. In addition, Zhu *et al.*[49] demonstrate a tunable microwave lens based on an array of cavities that can be filled with liquid metal using microfluidic technology and pneumatic valves. The lens shows an efficiency of 10% with a focal tunability of around 50%.

Many results are reported in the class of metalens based on *phase-change materials.*[50–54] Tunability of the focal length of around 10–15% is typically reported with a focusing efficiency of 20%. However, the transmitted intensity usually changes dramatically as the focal length is tuned. In the case of a heat-induced phase change, the metalens response time of 2 minutes is reported.[50]

For tunable metalenses based on *electrical control* of the chemical potential of graphene,[55–57] the focal length tunability of 10–20% is reported with efficiencies of 20–40%. The response time of such lenses is limited only by the switching time of a power supply, which can be on a microsecond scale. At the same time, for this class of lenses the operating frequency tunability is limited to some per cents as the operating frequency is set by the lens predefined geometry.

From the brief overview of the field, one can clearly see that the OML offers some advantages in terms of broad tunability of the focal length and operating frequency, wide operating bandwidth and high focusing efficiency. A very fast intrinsic response time of the OML is another intriguing feature interesting for ultrafast applications.

In summary, we introduced a concept of the magnetically tunable flat lens. It takes advantage of the resonant magnetic-field-dependent phase shift and features tunability by means of magnetic field control. We applied our model to a wide range of materials (semiconductors, graphene, ferrites and nanoparticle arrays), and found out that, with varying efficiency, the OML can be realised in a broad frequency range from microwaves to visible light. Moreover, using other magnetic field profiles, our OML can be reconfigured to operate as another optical component, *e.g.* as a beam deflector with a linear field profile or a grating with periodic field profile. We anticipate that the OML, based on available magneto-optical bulk and 2D materials, can find wide use in many optoelectronic technologies in a broad spectral range.

Conflicts of interest

There are no conflicts to declare.

Acknowledgements

We thank Prof. Oleg Kochukhov and Assoc. Prof. Vassilios Kapaklis (Uppsala University) for fruitful discussions, and Prof. Paolo Vavassori (CIC NanoGUNE).

V. G. acknowledges the support of Swedish Research Council (Vetenskapsrådet) (grant no. 2016-04593) and A. Y. N. acknowledges the Spanish Ministry of Science, Innovation and Universities (national project MAT2017-88358-C3-3-R) and Basque Department of Education (PIBA-2020-1-0014).

References

1 H. King, *The History of the Telescope*, Dover Publications, 2003.
2 B. E. Saleh and M. C. Teich, *Fundamentals of photonics*, John Wiley & Sons, 2019.
3 N. Yu, P. Genevet, M. A. Kats, F. Aieta, J.-P. Tetienne, F. Capasso and Z. Gaburro, Light Propagation with Phase Discontinuities: Generalized Laws of Reflection and Refraction, *Science*, 2011, **334**, 333–337.
4 L. Huang, X. Chen, H. Mühlenbernd, G. Li, B. Bai, Q. Tan, G. Jin, T. Zentgraf and S. Zhang, Dispersionless Phase Discontinuities for Controlling Light Propagation, *Nano Lett.*, 2012, **12**, 5750–5755.

 This journal is © The Royal Society of Chemistry 2021

Open Access Article. Published on 11 November 2020. Downloaded on 2/22/2021 9:58:49 AM.
This article is licensed under a Creative Commons Attribution-NonCommercial 3.0 Unported Licence.

5 P. Genevet, J. Lin, M. A. Kats and F. Capasso, Holographic detection of the orbital angular momentum of light with plasmonic photodiodes, *Nat. Commun.*, 2012, **3**, 1278.
6 F. Aieta, P. Genevet, M. A. Kats, N. Yu, R. Blanchard, Z. Gaburro and F. Capasso, Aberration-Free Ultrathin Flat Lenses and Axicons at Telecom Wavelengths Based on Plasmonic Metasurfaces, *Nano Lett.*, 2012, **12**, 4932–4936.
7 X. Chen, L. Huang, H. Mühlenbernd, G. Li, B. Bai, Q. Tan, G. Jin, C.-W. Qiu, S. Zhang and T. Zentgraf, Dual-polarity plasmonic metalens for visible light, *Nat. Commun.*, 2012, **3**, 1198.
8 A. Pors, M. G. Nielsen, R. L. Eriksen and S. I. Bozhevolnyi, Broadband Focusing Flat Mirrors Based on Plasmonic Gradient Metasurfaces, *Nano Lett.*, 2013, **13**, 829–834.
9 N. Yu and F. Capasso, Flat optics with designer metasurfaces, *Nat. Mater.*, 2014, **13**, 139–150.
10 F. Capasso, The future and promise of flat optics: a personal perspective, *Nanophotonics*, 2018, **7**, 953–957.
11 D. J. Coleman, Unified model for accommodative mechanism, *Am. J. Ophthalmol.*, 1970, **69**, 1063–1079.
12 E. Arbabi, A. Arbabi, S. M. Kamali, Y. Horie, M. Faraji-Dana and A. Faraon, MEMS-tunable dielectric metasurface lens, *Nat. Commun.*, 2018, **9**, 812.
13 S. M. Kamali, E. Arbabi, A. Arbabi and A. Faraon, A review of dielectric optical metasurfaces for wavefront control, *Nanophotonics*, 2018, **7**, 1041–1068.
14 A. She, S. Zhang, S. Shian, D. Clarke and F. Capasso, 2017 Conference on Lasers and Electro-Optics (CLEO), 2017, pp. 1–1.
15 A. She, S. Zhang, S. Shian, D. R. Clarke and F. Capasso, Large area metalenses: design, characterization, and mass manufacturing, *Opt. Express*, 2018, **26**, 1573.
16 S. M. Kamali, E. Arbabi, A. Arbabi, Y. Horie and A. Faraon, Highly tunable elastic dielectric metasurface lenses, *Laser Photonics Rev.*, 2016, **10**, 1002–1008.
17 H.-S. Ee and R. Agarwal, Tunable Metasurface and Flat Optical Zoom Lens on a Stretchable Substrate, *Nano Lett.*, 2016, **16**, 2818–2823.
18 A. She, S. Zhang, S. Shian, D. R. Clarke and F. Capasso, Adaptive metalenses with simultaneous electrical control of focal length, astigmatism, and shift, *Sci. Adv.*, 2018, **4**, eaap9957.
19 S. Colburn, A. Zhan and A. Majumdar, Tunable metasurfaces via subwavelength phase shifters with uniform amplitude, *Sci. Rep.*, 2017, **7**, 40174.
20 J. Sautter, I. Staude, M. Decker, E. Rusak, D. N. Neshev, I. Brener and Y. S. Kivshar, Active Tuning of All-Dielectric Metasurfaces, *ACS Nano*, 2015, **9**, 4308–4315.
21 S.-Q. Li, X. Xu, R. M. Veetil, V. Valuckas, R. Paniagua-Domínguez and A. I. Kuznetsov, Phase-only transmissive spatial light modulator based on tunable dielectric metasurface, *Science*, 2019, **364**, 1087–1090.
22 A. L. Holsteen, A. F. Cihan and M. L. Brongersma, Temporal color mixing and dynamic beam shaping with silicon metasurfaces, *Science*, 2019, **365**, 257–260.
23 F. Ding, Y. Yang and S. I. Bozhevolnyi, Dynamic Metasurfaces Using Phase-Change Chalcogenides, *Adv. Opt. Mater.*, 2019, **7**, 1801709.
24 Q. He, S. Sun and L. Zhou, Tunable/Reconfigurable Metasurfaces: Physics and Applications, *Research*, 2019, **2019**, 1–16.
25 T. H. Stix, *Waves in plasmas*, Springer Science & Business Media, 1992.
26 A. Siegman, *Lasers*, University Science Books, 1986.
27 S. Maier, *Handbook of Metamaterials and Plasmonics, World Scientific*, 2016, vol. 4.
28 M. Born and E. Wolf, *Principles of optics: electromagnetic theory of propagation, interference and diffraction of light*, Elsevier, 2013.
29 V. Nikolskiy and T. Nikolskaya, *Electrodynamics and radio wave propagation*, Nauka Publ., 1989, p. 508.
30 J. Bergman, The magnetized plasma permittivity tensor, *Phys. Plasmas*, 2000, **7**, 3476–3479.
31 M. Tymchenko, A. Y. Nikitin and L. Martín-Moreno, Faraday Rotation Due to Excitation of Magnetoplasmons in Graphene Microribbons, *ACS Nano*, 2013, **7**, 9780–9787.
32 D. Pozar, *Microwave Engineering*, Wiley, 4th edn, 2011.
33 S. Alberti, Plasma heating with millimetre waves, *Nat. Phys.*, 2007, **3**, 376–377.
34 External heating systems for ITER, 2019, https://www.iter.org/mach/Heating.
35 A. Ferreira, J. Viana-Gomes, Y. V. Bludov, V. Pereira, N. M. R. Peres and A. H. C. Neto, Faraday effect in graphene enclosed in an optical cavity and the equation of motion method for the study of magneto-optical transport in solids, *Phys. Rev. B: Condens. Matter Mater. Phys.*, 2011, **84**, 235410.
36 C. Hwang, D. A. Siegel, S.-K. Mo, W. Regan, A. Ismach, Y. Zhang, A. Zettl and A. Lanzara, Fermi velocity engineering in graphene by substrate modification, *Sci. Rep.*, 2012, **2**, 590.
37 P. R. Whelan, Q. Shen, B. Zhou, I. G. Serrano, M. V. Kamalakar, D. M. A. Mackenzie, J. Ji, D. Huang, H. Shi, D. Luo, M. Wang, R. S. Ruoff, A.-P. Jauho, P. U. Jepsen, P. Bøggild and J. M. Caridad, Fermi velocity renormalization in graphene probed by terahertz time-domain spectroscopy, *2D Mater.*, 2020, **7**, 035009.
38 N. Tang, B. Shen, M. Wang, Z. Yang, K. Xu, G. Zhang, T. Lin, B. Zhu, W. Zhou and J. Chu, Effective mass of the two-dimensional electron gas and band nonparabolicity in Al_x Ga_{1-x} N/Ga N heterostructures, *Appl. Phys. Lett.*, 2006, **88**, 172115.
39 T. Wang, X. Wang, Z. Chen, X. Sun, P. Wang, X. Zheng, X. Rong, L. Yang, W. Guo, D. Wang, *et al.*, High-Mobility Two-Dimensional Electron Gas at InGaN/InN Heterointerface Grown by Molecular Beam Epitaxy, *Adv. Sci.*, 2018, **5**, 1800844.
40 V. Agranovich, *Surface Polaritons*, Elsevier Science, 2012, pp. 47–52.
41 E. Palik and G. Ghosh, *Handbook of Optical Constants of Solids*, Elsevier Science, 1991, vol. 1, pp. 491–494.

Open Access Article. Published on 11 November 2020. Downloaded on 2/22/2021 9:58:49 AM.
This article is licensed under a Creative Commons Attribution-NonCommercial 3.0 Unported Licence.

42 A. Ciuciulkaite, K. Mishra, M. V. Moro, I.-A. Chioar, R. M. Rowan-Robinson, S. Parchenko, A. Kleibert, B. Lindgren, G. Andersson, C. Davies, A. Kimel, M. Berritta, P. M. Oppeneer, A. Kirilyuk and V. Kapaklis, Design of Amorphous Tb_xCo_{100-x} Alloys for All-Optical Magnetization Switching, *Phys. Rev. Mater.*, 2020, **4**, 104418.

43 R. M. Rowan-Robinson, J. Hurst, A. Ciuciulkaite, I.-A. Chioar, M. Pohlit, M. Zapata, P. Vavassori, A. Dmitriev, P. M. Oppeneer and V. Kapaklis, *Spectrally reconfigurable magnetoplasmonic nanoantenna arrays*, 2020, https://arxiv.org/abs/2005.14478.

44 I. Vlassiouk, P. Fulvio, H. Meyer, N. Lavrik, S. Dai, P. Datskos and S. Smirnov, Large scale atmospheric pressure chemical vapor deposition of graphene, *Carbon*, 2013, **54**, 58–67.

45 P. Salén, M. Basini, S. Bonetti, J. Hebling, M. Krasilnikov, A. Y. Nikitin, G. Shamuilov, Z. Tibai, V. Zhaunerchyk and V. Goryashko, Matter manipulation with extreme terahertz light: Progress in the enabling THz technology, *Phys. Rep.*, 2019, **836–837**, 1–74.

46 Z. Liu, Z. Liang, W. Tang and X. Xu, Design and fabrication of low-deformation micro-bolometers for THz detectors, *Infrared Phys. Technol.*, 2020, **105**, 103241.

47 J. Hebling, G. Almasi, I. Kozma and J. Kuhl, Velocity matching by pulse front tilting for large area THz-pulse generation, *Opt. Express*, 2002, **10**, 1161.

48 F. Callewaert, V. Velev, S. Jiang, A. V. Sahakian, P. Kumar and K. Aydin, Inverse-designed stretchable metalens with tunable focal distance, *Appl. Phys. Lett.*, 2018, **112**, 091102.

49 W. Zhu, Q. Song, L. Yan, W. Zhang, P.-C. Wu, L. K. Chin, H. Cai, D. P. Tsai, Z. X. Shen, T. W. Deng, S. K. Ting, Y. Gu, G. Q. Lo, D. L. Kwong, Z. C. Yang, R. Huang, A.-Q. Liu and N. Zheludev, A Flat Lens with Tunable Phase Gradient by Using Random Access Reconfigurable Metamaterial, *Adv. Mater.*, 2015, **27**, 4739–4743.

50 X. Yin, T. Steinle, L. Huang, T. Taubner, M. Wuttig, T. Zentgraf and H. Giessen, Beam switching and bifocal zoom lensing using active plasmonic metasurfaces, *Light: Sci. Appl.*, 2017, **6**, e17016–e17016.

51 W. Bai, P. Yang, S. Wang, J. Huang, D. Chen, Z. Zhang, J. Yang and B. Xu, Actively Tunable Metalens Array Based on Patterned Phase Change Materials, *Appl. Sci.*, 2019, **9**, 4927.

52 W. Bai, P. Yang, J. Huang, D. Chen, J. Zhang, Z. Zhang, J. Yang and B. Xu, Near-infrared tunable metalens based on phase change material $Ge_2Sb_2Te_5$, *Sci. Rep.*, 2019, **9**, 5368.

53 M. Y. Shalaginov, S. An, Y. Zhang, F. Yang, P. Su, V. Liberman, J. B. Chou, C. M. Roberts, M. Kang, C. Rios, Q. Du, C. Fowler, A. Agarwal, K. A. Richardson, C. Rivero-Baleine, H. Zhang, J. Hu and T. Gu, Reconfigurable all-dielectric metalens for diffraction-limited imaging, *Active Photonic Platforms*, 2020, **XII**, 114610M.

54 X. Li, S. Li, G. Wang, Y. Lei, Y. Hong, L. Zhang, C. Zeng, L. Wang, Q. Sun and W. Zhang, Tunable doublet lens based on dielectric metasurface using phase-change material, *Mod. Phys. Lett. B*, 2020, **34**, 2050313.

55 Z. Li, K. Yao, F. Xia, S. Shen, J. Tian and Y. Liu, Graphene Plasmonic Metasurfaces to Steer Infrared Light, *Sci. Rep.*, 2015, **5**, 12423.

56 Z. Wang, B. Hu, B. Li, W. Liu, X. Li, J. Liu and Y. Wang, Active focal control of an ultrathin graphene-metal metasurface lens, *Mater. Res. Express*, 2016, **3**, 115011.

57 P. Ding, Y. Li, L. Shao, X. Tian, J. Wang and C. Fan, Graphene aperture-based metalens for dynamic focusing of terahertz waves, *Opt. Express*, 2018, **26**, 28038.

This journal is © The Royal Society of Chemistry 2021